Emergent spin accumulation in non-Hermitian altermagnets

J. H. Correa [1,*] M. P. Nowak [2] and A. Pezo [3,†]
[1] Universidad Tecnológica del Perú, Dirección de Investigación Región Sur, Lima, Peru
[2] AGH University of Krakow, Academic Centre for Materials and Nanotechnology, al. A. Mickiewicza 30, 30-059 Krakow, Poland
[3] Institute for Solid State Physics, University of Tokyo, Kashiwa 277-8581, Japan

(Received 9 March 2026; revised 29 July 2026; accepted 31 July 2026; published 24 August 2026)

The recent interest in non-Hermitian systems has significantly broadened their application across condensed-matter physics, offering a unique framework to explore out-of-equilibrium phenomena. Simultaneously, altermagnets have emerged as a distinct magnetic class, characterized by unconventional spin-split bands protected by crystal symmetries. In this work, we investigate the interplay between non-Hermitian dynamics and spin transport in these materials, focusing on the Edelstein effect. We demonstrate that the introduction of non-Hermiticity in d-wave altermagnets and p-wave unconventional magnets opens novel susceptibility components that are inaccessible in Hermitian counterparts. Fundamentally, the dissipation breaks standard momentum selection rules, dynamically converting previously asymmetric channels into even-parity configurations under spatial inversion to allow macroscopic spin accumulation. Crucially, our results show that this nonconservative nature leads to the selective gain and loss of specific spin components, which can be finely tuned by the interplay between dissipation, the magnetic order parameter, and the Néel vector orientation. This phenomenon provides a new route for manipulating spin degrees of freedom through controlled nonconservative processes in emerging unconventional magnetic materials.

DOI: 10.1103/pcrs-tkry

I. INTRODUCTION

Altermagnets (AMs), a new magnetic phase with coexisting ferromagnetic and antiferromagnetic properties and spin polarization but zero net magnetization, has drawn attention as candidates for next-generation superconducting spintronic devices and for having promising applications in areas such as valleytronics, conductivity, and straintronics [1–3]. Within this framework, compounds such as CrSb, MnTe, and Mn_5Si_3, $V_2(Se,Te)_2O$ have been theoretically and experimentally identified as hosting remarkable altermagnetic signatures [4,5], including the strain-driven anomalous Hall effect and the efficient generation of spin currents via spin-orbit torques [6,7], linear and nonlinear Edelstein effects [8–12], topological superconductivity [13–15], Josephson properties and the diode effect [16–19], and quantum transport [20,21]. Beyond conventional AMs, recent studies on p-wave unconventional magnets (UMs) have revealed intriguing properties arising from their preserved time-reversal symmetry and broken inversion symmetry—features that clearly distinguish them from AM materials [22,23]. Notably, phenomena such as the emergence of the finite out-of-plane Edelstein effect [24,25], unique transport properties in hybrid systems [26–28], and unconventional superconductivity [29–31] have gained significant attention. The emergence of out-of-plane spin polarization, also referred to as the nonrelativistic Rashba-Edelstein effect, arises without requiring strong spin-orbit coupling (SOC), in contrast to the spin-momentum locking at the Fermi surface in typical ferromagnetic/heavy metal interfaces [32]. Instead, in p-wave magnets, a similar effect occurs due to the magnetic order, that is, in such a case the exchange field part of the Hamiltonian, e.g., $H_{xc}(\mathbf{k}) \propto t_i k_i$, directly mimics Rashba-like spin-momentum locking. A charge current, therefore, shifts the electronic distribution asymmetrically in momentum space, which generates nonequilibrium spin density even in systems without strong SOC [24,25]. However, despite this progress, the properties of AMs (UMs) are still largely restricted to their Hermitian features, effectively treating these systems as closed and dissipationless. Indeed, devices made of these structures operate in open environments, where coupling to external leads, disorder, and finite quasiparticle lifetimes are unavoidable [33]. These effects naturally introduce gain and loss processes, where a non-Hermitian (NH) description is necessary.

The inclusion of NH effects has emerged as a promising avenue for exploring unconventional topological phases that are markedly different from their Hermitian counterparts [34]. These effects provide a realistic description of systems characterized by energy gain and loss, leading to complex energy spectra and new phenomena under boundary conditions [35]. In particular, eigenstates can exhibit strong localization, a phenomenon known as the NH skin effect [36–40]. Furthermore, NH systems feature exceptional points (EPs), where eigenvalues and eigenstates coalesce—this is a fundamental aspect of NH physics [35,41,42]. Recently, EPs were identified in d-wave altermagnets coupled to ferromagnetic (FM) leads,

*Contact author: jorgehuamani90@gmail.com
†Contact author: apezol@issp.u-tokyo.ac.jp

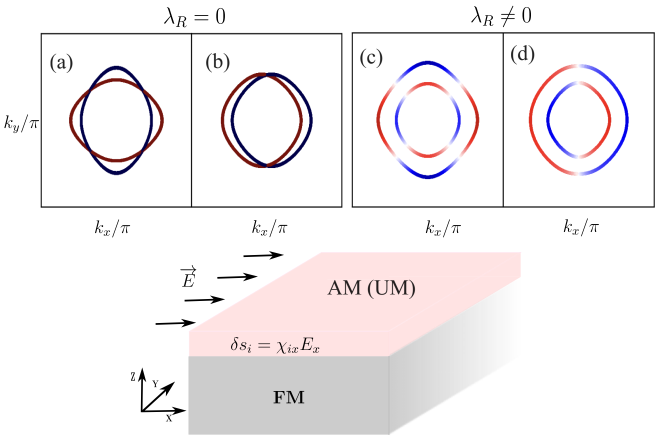

FIG. 1. Top panel: Fermi surfaces of the $d_{x^2-y^2}$ AM [(a),(c)] and p_x UM [(b),(d)], shown both in the absence and presence of Rashba SOC, respectively; color maps represent the spin expectation value $\langle s_z \rangle$. Bottom panel: Schematic representation of the in-plane electric field effect at the AM(UM)/FM lead interface. The diagram illustrates the coupling between the external electric field $\vec{E}$ and the interface formed by a ferromagnetic lead (FM) and an AM or UM (pink layer). The electric field in the $\hat{x}$ direction gives the spin accumulation in the i direction accordingly with $\delta s_i = \chi_{ix} E_x$.

tuned by external magnetic fields [43,44], and likewise in p-wave unconventional magnets [45,46]. Quantum transport studies within the NH framework have further revealed significant dissipation effects in the Hall conductance [47,48]. Such new concepts have led to an increasing interest in understanding how NH properties can be used to manipulate the spin degree of freedom. Advances in material growth and experimental techniques have enabled detailed exploration and utilization of spin dynamics. This can be probed by using spin-pumping techniques [49], exploiting the Seebeck effect [50], or by considering a less invasive approach, as is the case of THz emission in spintronic devices [51–53]. In particular, AMs (UMs), due to their anisotropic properties, offer an intriguing platform for the exploration of active spin-charge converters under various conditions. Their defining characteristic is that the conversion process does not depend on strong relativistic spin-orbit coupling [24], where collinear but alternating spin moments are responsible for mimicking the responses typically associated with heavy-element systems. This unique origin not only allows altermagnets to serve as efficient sources and detectors of spin currents, but it also embeds their functionalities in a manner that is dependent on crystal symmetry, leading to anisotropic and tunable effects [54].

In this work, we investigate the spin Edelstein effect within a NH framework given by the coupling of an AM(UM)/FM lead interface as depicted in the bottom panel of Fig. 1. By employing a tight-binding (TB) formalism, we extend linear-response theory to incorporate NH effects, identifying specific regions in phase space where the interplay between damping and gain yields experimentally accessible signatures. The structure of this article is as follows. In Sec. II, we introduce the TB model for the NH altermagnetic system and derive the susceptibility tensors using the Kubo formalism and Green's function techniques. In Sec. III, we discuss the impact of Néel vector orientation and vertex corrections on our results. Finally, Sec. IV summarizes our findings and provides concluding remarks.

II. THEORETICAL MODEL

A. Tight-binding Hamiltonian models

Non-Hermiticity provides a natural framework for describing open quantum systems where dissipation and finite quasiparticle lifetimes—inherent to most experimental setups—play a fundamental role. Here, following Ref. [41], we introduce NH features by interfacing an AM(UM) system with a FM lead, which acts as a dissipative environment. Such coupling in the wide-band limit is given by $\Sigma^R(\omega = 0) = -i\Gamma\sigma_0 - i\gamma\sigma_z$, where the first term is related to the orbital component and the second one to the spin components. The parameters $\Gamma = (\Gamma_\uparrow + \Gamma_\downarrow)/2$ and $\gamma = (\Gamma_\uparrow - \Gamma_\downarrow)/2$ characterize the average and imbalanced dissipation, respectively [41,55]. Likewise, the non-Hermitian parameters must satisfy $\Gamma \geqslant \gamma \geqslant 0$ in order to preserve causality and guarantee a physically stable dissipative state [56]. Furthermore, $\Gamma_\sigma = \pi(t')^2 \rho_L^\sigma$, where t' is the value of the interfacial coupling in the ferromagnetic lead, and ρ_L^σ is the spin-dependent surface density of states. Finally, σ_0 and σ_z denote the identity and z-component Pauli matrices.

The resulting NH Hamiltonian is defined as $H_{NH} = H_H + \Sigma(\omega = 0)$, where the Hermitian part $H_H = H_K + H_R + H_{AL}$ includes kinetic energy, Rashba SOC, and and AM(UM) contribution, respectively. The TB Hamiltonians of kinetic and Rashba SOC terms in reciprocal space are given by

$$\begin{aligned} H_K(\mathbf{k}) &= -2t(\cos k_x + \cos k_y)\sigma_0 - \mu\,\sigma_0, \\ H_R(\mathbf{k}) &= \lambda_R(\sin k_y\,\sigma_x - \sin k_x\,\sigma_y), \end{aligned} \tag{1}$$

where t is the hopping parameter, μ is the chemical potential, and λ_R represents the Rashba SOC parameter. For the altermagnetic sector, we adopt the following d-wave and p-wave Hamiltonians:

$$\begin{aligned} H_{AL}^d(\mathbf{k}) &= \alpha[2\sin k_x \sin k_y \sin 2\theta \\ &\quad + (\cos k_x - \cos k_y)\cos 2\theta](\mathbf{n}\cdot\sigma), \\ H_{UM}^p(\mathbf{k}) &= [t_x \sin k_x + t_y \sin k_y](\mathbf{n}\cdot\sigma). \end{aligned} \tag{2}$$

H_{AL}^d describes a d-wave altermagnet with strength α, where the orientation angle θ interpolates between $d_{x^2-y^2}$ $(\theta = 0)$ and d_{xy} $(\theta = \pi/4)$ symmetries [2,57,58]. Similarly, H_{UM}^p represents a p-wave unconventional magnet [26,29] with strengths t_x and t_y along the p_x and p_y symmetries, respectively. While we focus on this specific representation, we note that alternative formulations for odd-parity magnets have recently been proposed, such as the sublattice-based model in [59], which offers a complementary framework for studying emergent magnetic phases. Moreover, such a sublattice degree of freedom should be important to distinguish the localization of corner states as a result of non-Hermitian effects of the system [60]. In both models, $\mathbf{n}$ denotes the orientation of the Néel vector [25]. The top panel of Fig. 1 compares the Fermi surfaces of the Hermitian AM and UM systems in the absence [(a),(b)] and presence [(c),(d)] of Rashba SOC, while the bottom panel depicts the setup used in the model. For both $d_{x^2-y^2}$-wave AM and p_x-wave UM, turning on Rashba SOC with $n = (0, 0, 1)$ lifts the point degeneracies [(b),(d)], resulting in two separate, nonintersecting Fermi contours.

B. Kubo formula extension for spin dynamics

To investigate the out-of-equilibrium spin accumulation properties, we employ linear-response theory. Within this framework, the electrical driven spin accumulation arises as the response to an applied in-plane electric field E_j defined by the relation $\langle \delta\hat{s}_i\rangle = \sum_j \chi_{ij}E_j$. Using the Kubo formalism, the proportionality constant χ_{ij}, also known as the spin Edelstein susceptibility tensor, can be written as [61–64]

$$\chi_{ij} = -\frac{e\hbar}{8\pi}\int \partial_\epsilon f(\epsilon)\, d\epsilon\ \mathrm{Re}[\mathrm{Tr}\{\hat{v}_i(G^{R-A}(\mathbf{k},\varepsilon))\hat{\sigma}_j \times (G^{R-A}(\mathbf{k},\varepsilon))\}]. \tag{3}$$

Here, $G^{R\pm A} = G^R \pm G^A$, where G^R and G^A denote the retarded and advanced Green's functions (GFs), respectively. Similarly, $\hat{v}_i = \partial_{k_i}H_{NH}(\mathbf{k})$ and $\hat{\sigma}_j$ represent the momentum-dependent velocity and spin matrices. The term $f(\epsilon)$ denotes the Fermi-Dirac distribution, and Tr indicates the trace over the internal degrees of freedom. Moreover, we restrict our analysis to the low-temperature limit ($T \to 0$), where the derivative of the distribution function reduces to a delta function, $\partial_\epsilon f(\epsilon) \to \delta(\epsilon-\mu)$. In terms of response symmetry, upon the action of time-reversal symmetry ($\mathcal{T}$), Eq. (3) is $\mathcal{T}$-even.

To incorporate non-Hermiticity arising from the coupling to the ferromagnetic lead, we adopt the biorthogonal basis formalism [47,48]. The retarded NH Green's function is expressed as

$$G^R(\mathbf{k},\varepsilon) = \frac{P_+(\mathbf{k})}{\varepsilon - E^R_+(\mathbf{k})} + \frac{P_-(\mathbf{k})}{\varepsilon - E^R_-(\mathbf{k})}. \tag{4}$$

Here, $P_\pm$ are the projection operators onto the eigenstates, defined as $P_\pm = |\Psi^R_\pm\rangle\langle\Psi^L_\pm|$, where $|\Psi^{R,L}_\pm\rangle$ denote the right (left) eigenvectors obtained from our NH Hamiltonian satisfying the biorthogonal condition $\langle\Psi_m||\Psi_n\rangle = \delta_{nm}$ with $\sum_\pm P_\pm = \sigma_0$ [48], and $E^R_\pm$ are the corresponding complex energies obtained from the NH Hamiltonian. The integrand is performed over the BZ, and we only take the real part of the susceptibility tensor. From Eq. (4), the advanced GF is given by $G^A = [G^R]^\dagger$. In the Hermitian limit $\Sigma^R(\omega=0) \to 0$, the GF recovers their Hermitian form with $|\Psi^R_\pm\rangle = |\Psi^L_\pm\rangle$.

III. RESULTS

In this section, we investigate the field-driven spin accumulation considering an external electric field applied along the x direction, i.e., $\mathbf{E} = E_x\hat{x}$, to the system defined by the AM(UM)/ FM lead coupling (see Fig. 1). Specifically, we calculate the spin accumulation along the j direction, given by Eq. (3). The real part of the susceptibility tensor is expressed in units of $\chi_0 = e\hbar/\pi$, and unless otherwise specified, all numerical TB simulations are performed considering the hopping amplitude, t, as a scale of energy. Specifically, we set the energy scale by fixing $t = 0.5$ eV, with $\lambda_R = 0.6t$ and $\mu = 0$. On the other hand, to support our findings, we supplement our simulations with analytical derivations of the quantum-mechanical trace from Eq. (3) using low-energy effective models for both the AM(UM) phases. Furthermore, the role of disorder is discussed by means of the vertex correction, showing a small impact given the details of the considered system Hamiltonian; the details are given in Appendix B.

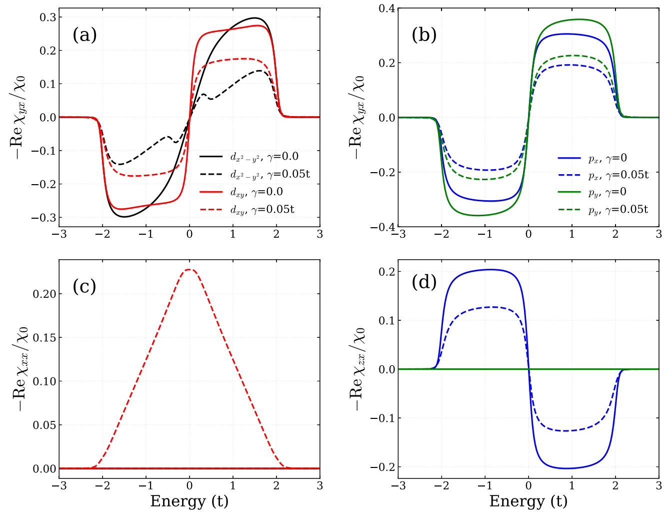

FIG. 2. Real part of the spin susceptibility tensor for a NH system with the Néel vector along the z direction. Left panel [(a),(c)]: d-wave AM; right panel [(b),(d)] : p-wave UM. The transversal component χ_{yx} [(a) and (b)] decreases for $\gamma \neq 0$ while the diagonal component χ_{xx} arises for d_{xy} wave (c) and an out-of plane component χ_{xz} decreases by the action of γ (d). For (a) and (c), $\alpha = 0.2t$, while for (b) and (d), $t_x = 0.2t$, $t_y = 0$ and $t_x = 0$, $t_y = 0.2t$ for p_x and p_y, respectively.

A. Out-of-plane Néel order n ‖ z direction

In Fig. 2, we present the corresponding components of the spin Edelstein spin susceptibility responses for d-wave [(a),(c)] and p-wave [(b),(d)] symmetries in left and right panels respectively, considering a Néel vector oriented along the z direction, i.e., $\mathbf{n} = (0, 0, 1)$. The Hermitian case is represented by solid curves ($\Gamma = \gamma = 0$), while the NH regime is represented by dashed curves with $\Gamma = \gamma = 0.05t$. While the high values of Rashba SOC and AM(UM) parameters are selected to provide computational clarity and visually resolve the non-Hermitian topological features across the full Brillouin zone maps, this choice represents a weak-coupling dissipative perturbation regime (γ much smaller than t), which aligns with previous studies [41,56]. Focusing first on the d-wave AM, the transversal in-plane susceptibility χ_{yx} exhibits an almost oscillatory behavior that is symmetric around $E = 0$. While this response—enhanced by Rashba SOC—is consistent with recent reports [10,24], the symmetry $C_{4z}\mathcal{T}$ ensures that both the longitudinal (χ_{xx}) and out-of-plane (χ_{zx}) components vanish. Revisiting it here is instructive, as its physical origin becomes especially transparent in the NH regime.

The inclusion of non-Hermiticity, controlled by the parameters γ and Γ, modifies the intensity of χ_{yx}, as evidenced by the dashed curves. For the d-wave case, the magnitude of the susceptibility is progressively reduced as γ increases. This suppression signals dissipative effects characteristic of NH quantum transport [47,65]. Remarkably, non-Hermiticity qualitatively alters the symmetry-imposed absence of longitudinal components. As shown in Fig. 2(c), a finite longitudinal in-plane response χ_{xx} emerges for the d_{xy} altermagnet (red dashed curve) upon activating γ. Unlike the dissipative suppression observed in χ_{xx}, the χ_{xx} signal is significantly enhanced with increasing γ. This behavior stems from a NH spin-filtering mechanism, where the spin-asymmetric imaginary self-energy yields heavily differential dissipation rates for the two spin channels ($\Gamma_\uparrow \neq \Gamma_\downarrow$). Rather than invoking an active quantum gain, the complex self-energy selectively broadens and suppresses the spectral weight of one spin species while leaving the opposite channel unaffected. In a steady-state driven scenario, this massive lifetime contrast prevents the mutual cancellation of the altermagnetic bands, effectively purifying the net spin accumulation via differential decay. The emergence of this component can be understood through the momentum parity of the integrand within the BZ, as will be shown in Sec. III C 1, in which we consider the effective models of our TB Hamiltonians. In the d_{xy} case, the product of the momentum-dependent velocities and the altermagnetic order parameter—proportional to $\sin k_x \sin k_y$ —acquires an overall even parity only in the presence of the NH coupling γ. Consequently, the integration yields a nonvanishing contribution and therefore a finite χ_{xx} response. In contrast, for the $d_{x^2-y^2}$ symmetry, the mismatch between the velocity vectors (which in this case is proportional to $\sin k_x$ (odd function)] and the d-wave AM form factor preserves the null response, even in the NH regime. On the other hand, the out-of-plane component χ_{zx} is negligible compared to χ_{xx}, which appears three orders of magnitude lower and only with large values of NH parameters (not shown here).

We now turn our attention to the p-wave UM. Similar to the d-wave AM, the system exhibits finite χ_{yx}, which decreases with the action of γ [see Fig. 2(b)]. In contrast, the p_x UM shows a finite χ_{zx} even in the Hermitian regime, as shown in Fig. 2(d) by the blue solid curve, which agrees with Ref. [25]. Upon increasing γ, this response is progressively suppressed, as indicated by the blue dashed curve, displaying a dissipative behavior similar to that observed for χ_{yx}. Symmetry considerations dictate that the induced spin accumulation along the z-axis is highly sensitive to the p-wave orientation relative to the electric field direction. Specifically, for an electric field applied along the x-direction (E_x), the response coefficient χ_{zx} is finite for the p_x symmetry but vanishes identically for p_y, which will be show in Sec. III C 3. This vanishing occurs because the orthogonal alignment between the field E_x and the p_y anisotropy axis preserves a parity symmetry that causes the spin contributions to cancel out upon integration over the Fermi surface. Conversely, if the field is applied along the y-direction (E_y), the response χ_{zy} becomes finite for the p_y channel while the p_x contribution is null, a selection rule that remains robust even in the Hermitian limit [25]. Notably, while the NH imbalance dissipation γ induces a spin population in the d-wave regime, it is insufficient to break the structural parity constraints in the p-wave sector, leaving these orthogonal null responses unaffected.

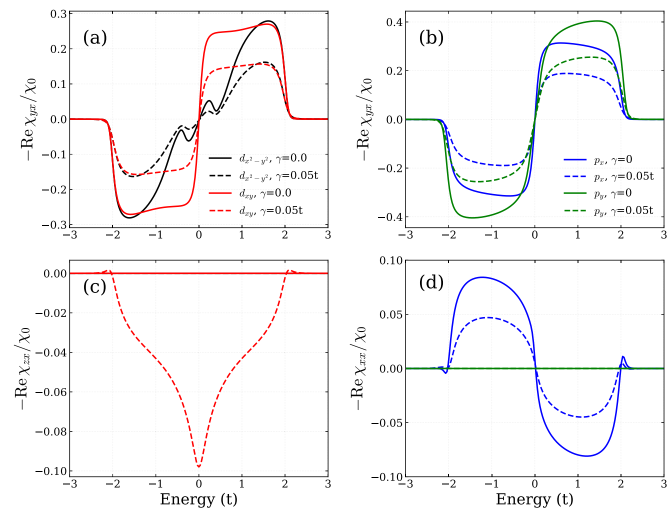

FIG. 3. Real part of the spin susceptibility components for a non-Hermitian systems with the Néel vector along the x direction. Left panel: d-wave AM [(a),(c)]; right panel: p- wave UM [(b),(d)]. The transversal component χ_{yx} [(a) and (b)] decreases for $\gamma \neq 0$, the finite out-of-plane component χ_{xz} arises for d_{xy} wave (c), and the longitudinal component χ_{xx} decreases by the action of γ (d). For (a) and (c), $\alpha = 0.2t$, while for (b) and (d), $t_x = 0.2t, t_y = 0$ and $t_x = 0, t_y = 0.2t$ for p_x and p_y, respectively.

B. In-plane Néel configurations n $\parallel x, y$

After discussing the classic Néel vector orientation, we move to the Néel vector oriented along the x direction $\mathbf{n} = (1, 0, 0)$. In Fig. 3, we plot the susceptibility components for d-wave AM [(a),(c)] and p-wave UM [(b),(d)] in the left and right panels, respectively. Similar to the previous case, the transversal in-plane component χ_{yx} exhibits an almost oscillatory behavior in both systems, with its magnitude decreasing as γ increases, as shown in panels (a) and (b).

Focusing on the d-wave AM and in the Hermitian limit, the components χ_{xx} and χ_{zx} vanish, where the rotation symmetry is still preserved even for different Néel vectors. In contrast, in this case, the component χ_{zx} emerges in the NH regime only on the d_{xy}-wave AM, as illustrated by the dashed red curve in panel (c). This can be understood as the NH term produces a spin torque where the altermagnet parameter competes directly with the Rashba SOC parameter and the term coupled with σ_z is purely imaginary, $\sim i\gamma$. This term gives an even parity in the integrand and therefore induces non-zero values of χ_{zx}.

Regarding the p-wave symmetry, the χ_{yx} signal decreases with increasing γ, mirroring the dissipative trend observed in the d-wave case. However, a key distinction arises in the χ_{zx} component only for p_x-wave AM, which is already finite in the Hermitian regime [Fig. 3(d), blue solid curve], consistent with Ref. [25]. In this sector, the NH term acts primarily as a dissipator, progressively suppressing the signal intensity (blue dashed curve). This contrast with the d-wave AM case—where NH terms act as a generative mechanism for new components—can be understood through the parity

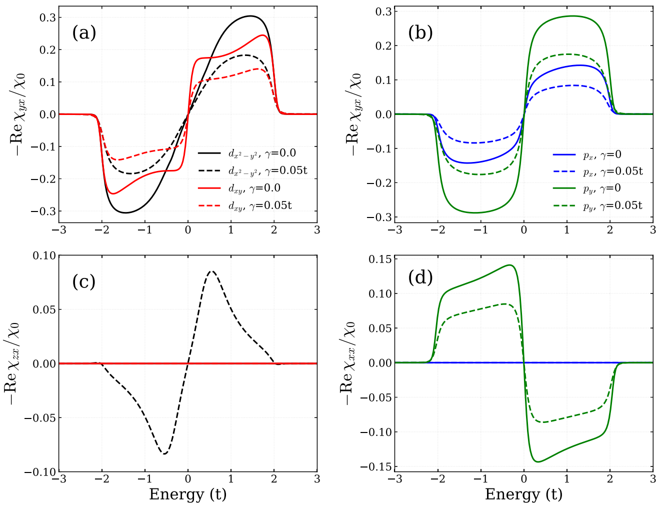

FIG. 4. Real part of the spin susceptibility components for a non-Hermitian systems with the Néel vector along the y direction. Left panel [(a),(c)]: d-wave AM; right panel [(b),(d)]: p-wave UM. The transversal component χ_{yx} [(a) and (b)] decreases for $\gamma \neq 0$, the finite out-of-plane component χ_{zx} arises for the $d_{x^2-y^2}$ wave (c), and the longitudinal component χ_{xx} for p_y decreases by the action of γ (d). For (a) and (c), $\alpha = 0.2t$, while for (b) and (d), $t_x = 0.2t, t_y = 0$ and $t_x = 0, t_y = 0.2t$ for p_x and p_y, respectively.

of the orbital form factors. The p_x symmetry possesses odd parity in only one momentum direction; consequently, the overall parity of the integrand is determined by the remaining velocity and spin operators, which allows for a nonvanishing integral even without the NH framework. In contrast, the d_{xy} symmetry ($\propto \sin k_x \sin k_y$) is odd in both directions, enforcing a global cancellation in the Hermitian limit that can only be lifted by the complex spectral redistribution induced by γ. On the other hand, the situation undergoes a significant change when the Néel vector is oriented along the y-direction, i.e., $\mathbf{n} = (0, 1, 0)$, as illustrated in Fig. 4. Similar to the previous case, the χ_{yx} component in both d-wave AM and p-wave UM systems [(a) and (b)] exhibits a symmetric, oscillatory-like profile whose magnitude is progressively suppressed by γ. This confirms that the χ_{xy} response remains robust and finite regardless of the Néel vector orientation. However, the NH coupling γ induces a qualitative change in the other susceptibility components. Specifically, for $\hat{\mathbf{n}} \parallel y$, the $d_{x^2-y^2}$ altermagnet exhibits the emergence of a finite χ_{zx} response in the NH regime [Fig. 4(c)]. Remarkably, χ_{zx} remains vanishingly small for this symmetry, indicating that the y-axis orientation shifts the NH-induced activation exclusively to the collinear sector for the $d_{x^2-y^2}$ symmetry. On the other hand, the y-orientation leads to a finite χ_{xx} in the p_y-wave UM even in the Hermitian limit, as indicated by the solid green curve in (d); this result is in good agreement with Ref. [25]. The intensity of this component decreases with increasing γ, as shown by the green dashed curve.

C. Analysis of the effective Hamiltonian

In this section, we derive an analytical expression for the trace of the response susceptibility matrix defined in Eq. (3). To simplify the calculations, we will employ the effective models of Eqs. (1) and (2) within a $\mathbf{k}\cdot\mathbf{p}$ approximation. Furthermore, we examine the resulting momentum-space spin textures, specifically characterizing their behavior within the NH regime, to assess the impact of dissipation on the spin accumulation. Throughout this analysis, we focus on the configuration where the Néel vector is aligned along the z axis; however, the formal framework presented here is general, and extending the analysis to other Néel vector orientations is straightforward.

1. Spin accumulation for d_{xy}-wave AM and out-of-plane Néel order in the $\mathbf{n} \parallel z$ direction

To demonstrate the emergence of χ_{xx} for the d_{xy}-wave AM, we computed the effective retarded GF of a two-level system [66], which is given by

$$G^R_{kp}(\mathbf{k}, E) = [(E + i\eta)\mathbb{I} - H_{kp}]^{-1}, \tag{5}$$

where η is the broadening, and the two-level $\mathbf{k}\cdot\mathbf{p}$ Hamiltonian can be written as $H_{kp} = d_0\sigma_0 + \mathbf{d}\cdot\sigma$, where

$$d_x = \lambda_R k_y, \quad d_y = -\lambda_R k_x, \quad d_z^{\theta=\pi/4} = 2\alpha k_x k_y - i\gamma. \tag{6}$$

Based on [67], we can find an analytical expression for G^R that can be written as

$$G^R_{kp}(\mathbf{k}, \varepsilon) = \frac{\varepsilon\mathbb{I} + \mathbf{d}.\sigma}{\varepsilon^2 - d^2}, \tag{7}$$

where $\varepsilon = E + i\eta$ and $d = \sqrt{d_x^2 + d_y^2 + d_z^2}$. After some algebraic steps, the effective retarded GF can be expressed as

$$G^R_{kp}(\mathbf{k}, E) = \frac{1}{D(\mathbf{k})}\begin{bmatrix} -2\alpha k_x k_y - i(\eta - \gamma) - E & -\lambda_R(ik_x + k_y) \\ \lambda_R(ik_x - k_y) & 2\alpha k_x k_y - i(\eta + \gamma) - E \end{bmatrix}, \tag{8}$$

with $D(\mathbf{k}) = \lambda^2(k_x^2 + k_y^2) - (i\eta + E)^2 + (2\alpha k_x k_y - i\gamma)^2$. With this in hand, we can compute an analytical expression for the trace of the matrix in Eq. (3). For spin accumulation in the x direction and for momentum up to the second $O(\mathbf{k}^2)$ order, we obtain

$$\mathrm{Tr}^{d_{xy}}\{\hat{v}_x G^{R-A}(\mathbf{k}, E)\hat{\sigma}_x G^{R-A}(\mathbf{k}, E)\}_{kp} = \frac{\gamma\left(-192\alpha\eta k_x^2 k_y^2 \lambda_R^3 E - 64\alpha\eta k_y^2 \lambda_R E^3\right)}{-16\alpha^2 k_x^2 k_y^2 E^6 + 32\alpha\eta\gamma k_x k_y E^5 + \gamma^2 B + Q + E^8}, \tag{9}$$

where

$$B = -16\alpha^2 k_x^2 k_y^2 E^4 + 24 k_x^2 k_y^2 \lambda_R^4 E^2 - 12 k_x^2 \lambda_R^2 E^4 - 12 k_y^2 \lambda^2 E^4 + 4E^6,$$
$$Q = 12 k_x^2 k_y^2 \lambda^4 E^4 - 4 k_x^2 \lambda^2 E^6 - 4 k_y^2 \lambda^2 E^6. \tag{10}$$

This analytical expression reveals that the spin accumulation in the x-direction vanishes when $\gamma = 0$, a result consistent with our numerical TB calculations. However, for a finite NH coupling $\gamma \neq 0$, the NH terms break this symmetry, shifting the parity of the function to even and leading to the emergence of a finite χ_{xx} as derived in detail in Appendix A. A similar computation can be made by the $d_{x^2-y^2}$ altermagnetic channel, where in this case $d_z^{\theta=0} = \alpha(k_x^2 - k_y^2) - i\gamma$ in Eq. (6), and the corresponding trace is given by

$$\mathrm{Tr}^{d_{x^2-y^2}}\{\hat{v}_x G^{R-A}(\mathbf{k}, E)\hat{\sigma}_x G^{R-A}(\mathbf{k}, E)\}_{kp} = \frac{\gamma^2\left(64\alpha^2 k_x k_y^2 \lambda E^2 - 16\alpha k_x E^4\right) + \gamma H}{8\alpha^2 k_x^2 k_y^2 E^6 + \gamma^2 G + \gamma F + Q + E^8}, \tag{11}$$

where

$$H = 128\alpha^2 \eta k_x k_y^2 E^3 + 32\alpha\eta k_x k_y^2 \lambda_R^4 E - 32\eta k_x \lambda_R^2 E^3,$$
$$G = 8\alpha^2 k_x^2 k_y^2 E^4 + 24 k_x^2 k_y^2 \lambda^4 E^2 - 12 k_x^2 \lambda^2 E^4 - 12 k_y^2 \lambda^2 E^4 + 4E^6,$$
$$F = 16\alpha\eta k_x^2 E^5 - 16\alpha\eta k_y^2 E^5.$$

From this expression, it is straightforward to verify that the parity of the numerator is odd while the denominator is even; consequently, the entire trace behaves as an odd function of the momentum, ensuring that its integral over the BZ vanishes due to the symmetry. As demonstrated by our analytical results, we confirm the emergence of finite χ_{xx} in d_{xy} symmetry, which remains zero in $d_{x^2-y^2}$ symmetry. Furthermore, a key distinguishing feature is the requirement of a finite altermagnetic parameter α to obtain a nonvanishing trace in Eq. (9), which clearly differentiates this system from a conventional Rashba semiconductor.

2. *Spin accumulation for $d_{x^2-y^2}$-wave AM with Néel order in the $\mathbf{n} \parallel y$ direction*

To demonstrate the emergence of the out-of-plane spin accumulation, characterized by the response coefficient χ_{zx} in a $d_{x^2-y^2}$-wave AM with the Néel vector oriented along the y-direction, the second and third terms in Eq. (6) are modified as follows:

$$d_y^{\theta=0} = -\lambda_R k_x + \alpha\left(k_x^2 - k_y^2\right),$$
$$d_z = -i\gamma. \tag{12}$$

By computing the analytical trace for the out-of-plane spin accumulation under an applied electric field along the x-direction, we obtain the following expression:

$$\mathrm{Tr}^{d_{x^2-y^2}}\left\{\hat{v}_x G^R(\mathbf{k}, E)\hat{\sigma}_z G^A(\mathbf{k}, E)\right\}_{kp} = \frac{\gamma\left(64\alpha^2\eta k_x k_y^2 E^3 + 96\alpha\eta k_x^2 \lambda_R E^3 - 32\alpha\eta k_y^2 \lambda_R E^3 + M\right)}{8\alpha^2 k_x^2 k_y^2 E^6 - 8\alpha k_x k_y^2 \lambda_R E^6 + \gamma^2 P + Q + E^8}, \tag{13}$$

where

$$M = 32\eta k_x k_y^2 \lambda_R^4 E - 32\eta k_x \lambda_R^2 E^3,$$
$$P = 24\alpha^2 k_x^2 k_y^2 E^4 - 24\alpha k_x k_y^2 \lambda_R E^4 + 24 k_x^2 k_y^2 \lambda_R^4 E^2 - 12 k_x^2 \lambda_R^2 E^4 - 12 k_y^2 \lambda_R^2 E^4 + 4E^6.$$

A parity analysis of Eq. (13) under individual axial inversions ($k_x \to -k_x$, $k_y \to -k_y$) gives the physical mechanism behind the spin response. The lowest-order expansion of the denominator is dominated by the isotropic background $E^8 + Q$, which is even in momemtum $\mathbf{k}$. Crucially, the second ($96\alpha\eta k_x^2 \lambda_R^3 E$) and third ($-32\alpha\eta k_y^2 \lambda_R E^3$) monomials in the numerator possess full axial symmetry (even parity under both k_x and k_y). As a result, these terms completely survive in the standard cancellations on the Fermi surface. Furthermore, the asymmetric altermagnetic term in the denominator ($-32\alpha k_x k_y^2 \lambda_R E^6$), which is odd in k_x, dynamically couples with the remaining odd terms of the numerator via geometric series in a similar way to the previous section. This cross-coupling generates additional even-parity channels ($\propto k_x^2 k_y^4$) that reinforce the transport. This symmetry-lifting mechanism ensures that the full-zone integration of the integrand remains nonvanishing, establishing a robust and finite intrinsic spin accumulation coefficient χ_{zx} driven by the competition between the altermagnetic field and the NH parameter γ. A similar analysis for the d_{xy}-wave AM leads the response χ_{zx} to vanish in this case, in total agreement with the calculations of our TB formalism.

3. *Intrinsic out-of-plane response and dissipation-driven decay in the p_x-wave UM for Néel vector $\mathbf{n} \parallel z$*

Using Eq. (7), we can evaluate the dissipation-driven behavior of the response function χ_{zx} for the p_x-wave channel, where the corresponding orbital component is given by

$$d_z^{p_x} = t_x k_x - i\gamma. \tag{14}$$

Following the procedure outlined in the previous section and expanding the response function to linear order in the momentum coordinates around the high-symmetry points, we arrive at the momentum-space trace:

$$\mathrm{Tr}^{p_x}\{\hat{v}_x G^{R-A}(\mathbf{k},E)\hat{\sigma}_z G^{R-A}(\mathbf{k},E)\}_{kp} = \frac{-8\eta^2E^4 + \gamma\big(-32\eta k_x\lambda^2E^3 - 64\eta k_xE^3t_x^2\big) + \gamma^2\big(32\eta^2E^2t_x - 8E^4t_x\big)}{4\eta^2E^6 + 16\eta\gamma k_xE^5t_x + \gamma^2(4\eta^2E^4 + 4E^6) + E^8}. \quad (15)$$

This analytical expression explicitly confirms that in the Hermitian limit ($\gamma = 0$), the integrand reduces to a momentum-independent constant, yielding a finite and robust intrinsic spin accumulation upon integration over the Brillouin zone. Conversely, when dissipation is introduced ($\gamma \neq 0$), a systematic Taylor expansion shows that the first-order dissipative corrections $[O(\gamma^1)]$ in both the numerator and denominator are proportional to odd powers of momentum (k_x^1). Consequently, these linear-in-γ terms vanish identically due to parity constraints under the $k_x \to -k_x$ operation. The leading-order effect of dissipation manifests exclusively at the quadratic level $[O(\gamma^2)]$, where even-parity cross-products survive the integration, thereby driving the smooth decay of the intrinsic p_x response.

On the other hand, a similar analysis for the p_y-wave UM dictates that the corresponding effective field component along the z-direction is described by

$$d_z^{p_y} = t_yk_y - i\gamma. \quad (16)$$

By evaluating the symmetry of the resulting integrand under full-zone integration, the algebraic trace for the χ_{zx} response vanishes identically due to mutually destructive parity compensations between different quadrants of the Brillouin zone. Consequently, the explicit analytical expression for this channel is omitted here for brevity.

4. Spin expectation values for d_{xy} and p_x for the Néel vector in the $\mathbf{n} \parallel z$ direction

Although the biorthogonal approach could be used for these calculations, we will restrict our analysis to the right eigenstates as an approximation for small values of the NH parameters. The spin expectation values are defined as

$$S_i^{\pm} = \langle\psi_{\pm}|\,\sigma_i\,|\psi_{\pm}\rangle, \quad (17)$$

where $|\psi_{\pm}\rangle$ are the eigenstates of the $\mathbf{k}\cdot\mathbf{p}$ Hamiltonian. With this in hand, the expectation value components can be written as

$$S_x^{\pm} = 2|N|^2\mathrm{Re}[f_k^{\pm}], \quad S_y^{\pm} = 2|N|^2\mathrm{Im}[f_k^{\pm}],$$
$$S_z^{\pm} = |N|^2(1 - |f_k^{\pm}|^2), \quad (18)$$

where

$$|N|^2 = \frac{1}{1 + |f_k^{\pm}|^2}, \quad f_k^{\pm} = \frac{-d_z \pm d}{(d_x - id_y)}. \quad (19)$$

To visually unveil the microscopic mechanism behind the NH generation and modulation of spin transport, we plot the momentum-resolved spin texture differences, $S_i = S_i^+ - S_i^-$, across the full Brillouin zone in Fig. 5. The columns from left to right display the distributions for the ΔS_x, ΔS_y, and ΔS_z components, respectively, contrasting the altermagnetic d_{xy}-wave AM [top row, panels (a)–(c)] against the p_x-wave UM [bottom row, panels (d)–(f)]. The red and blue colors represent positive and negative values of the spin-texture differences, while the distinct white regions represent the exact momentum coordinates where the textures vanish or where the non-Hermitian EPs are located. For the d_{xy}-wave AM (top row), the NH effects introduce a clear distinction from the conventional Hermitian limit. In the standard Hermitian case, the only surviving transport channel is the transverse S_y response. Upon introducing the NH dissipative coupling, this intrinsic S_y component [panel (b)] persists but undergoes a noticeable reduction in magnitude due to environmental damping, leaving a wide white region centered around the origin where the EPs are located [44]. Crucially, the dissipation dynamically activates a novel longitudinal S_x response [panel (a)], which completely emerges as a direct consequence of the NH parity-lifting mechanism. The white sharp features at the boundaries of these lobes mark the boundaries of the exceptional structures where the complex energy gap closes. Meanwhile, the S_z component [panel (c)] remains strictly zero across the entire Brillouin zone due to the robust spin-locking enforced by the z-oriented Néel vector, preventing any out-of-plane spin accumulation. A contrasting behavior is manifested in the bottom row for the p_x-wave UM. In the Hermitian limit, this symmetry naturally supports finite responses in both the S_y and S_z channels. Under the influence of NH dissipation, both the intrinsic S_y [panel (e)] and S_z [panel (f)] persist, though their overall magnitudes are attenuated by the coupling to the open environment. Most notably, unlike the altermagnetic case, the longitudinal S_x component [panel (d)] never emerges in the p_x-wave phase, remaining entirely suppressed across the momentum space except for the sharp white nodal lines tracking the EPs [45]. In panel (f), the sharp white boundary at $k_x = 0$ perfectly separates the antisymmetric binary lobes of the S_z component, highlighting how the p_x-wave geometry locks the EPs to high-symmetry axes. This clear divergence between the d_{xy}-wave and p_x-wave symmetries demonstrates that NH dissipation can act either as an activation parameter for forbidden transport channels or as a controlled damping mechanism for existing ones, with the EPs leaving a clear topological fingerprint on the observable spin-charge conversion.

IV. CONCLUSIONS

We have investigated the interplay between altermagnetism (unconventional magnetism) and NH dynamics in the context of the Edelstein effect. By considering a hybrid system comprising an AM(UM) coupled to a ferromagnetic lead which acts as a dissipative environment, we have demonstrated that the dissipative landscape, introduced via complex self-energies, acts as a symmetry-selective filter for spin-charge conversion. Our results reveal that while the transversal in-plane components of the spin susceptibility undergo significant damping due to the NH terms in both d-wave and p-wave symmetries, this dissipation facilitates a nontrivial

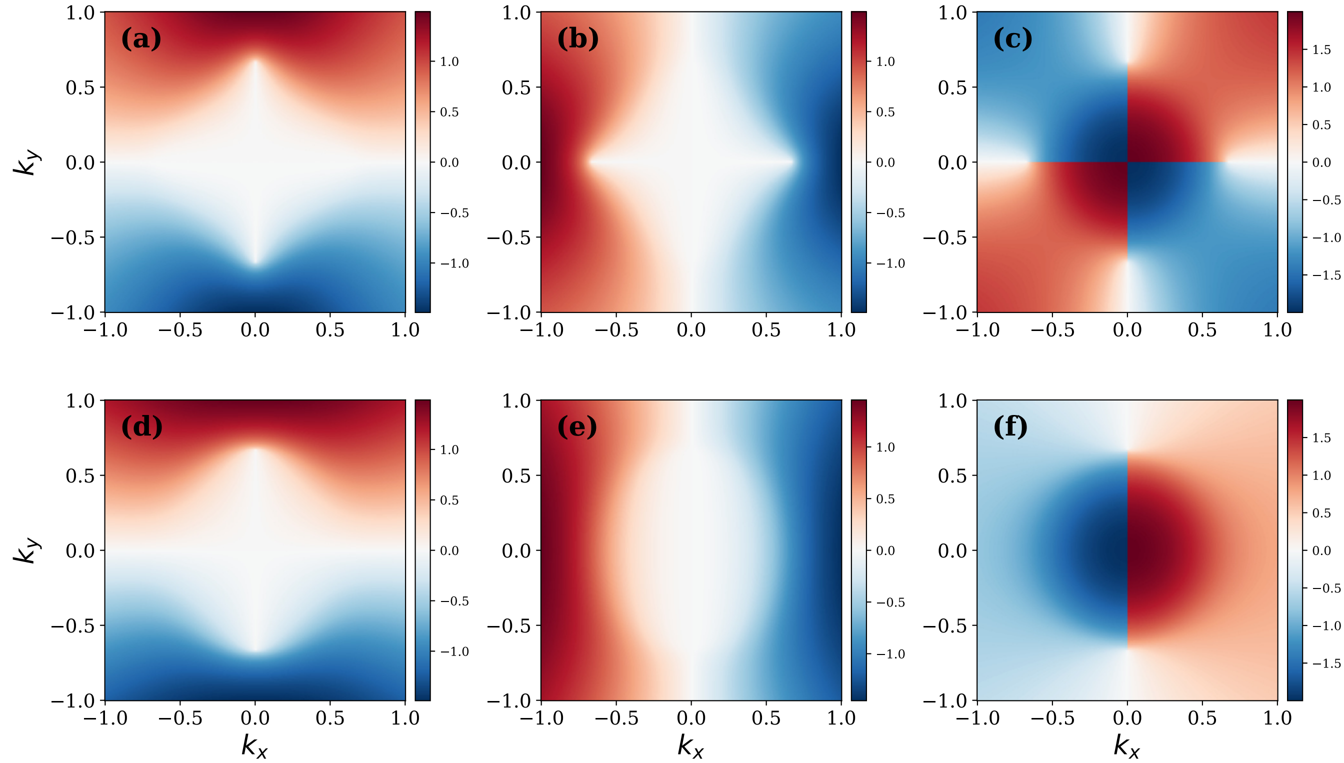

FIG. 5. Momentum-resolved spin texture differences ($\Delta S_i = S_i^+ - S_i^-$) for d_{xy}-wave AM (a)–(c) and p_x-wave UM (d)–(f) models with the Néel vector along the z direction. From left to right, the columns represent ΔS_x (a),(d), ΔS_y (b),(e), and ΔS_z (c),(f), respectively. The white regions highlight the nodal lines and the positions of non-Hermitian exceptional structures

redistribution of the spin accumulation. Specifically, in the d-wave AM, we find the emergence of finite longitudinal and out-of-plane susceptibility components that are otherwise suppressed in the Hermitian case. Moreover, these components arise for specific Néel vector orientations; in particular, the emergence of the diagonal component χ_{xx} for the d_{xy}-wave AM requires a finite altermagnetic parameter α, which underscores the fundamental difference between this system and a conventional Rashba semiconductor. This phenomenon suggests that non-Hermiticity can be exploited to manipulate the spin-texture orientation in AMs, offering new knobs for realizing chiral spin-orbitronic features in dissipative quantum regimes such as in spin-orbit torque measurements and THz spintronics emitters. Physically, this entire NH system leading to emergence or dissipative behavior is structurally rooted in the modification of the momentum parity selection rules under dissipative perturbations; the interplay between the parameter γ and the magnetic order parameters dynamically lifts the standard geometric cancellations by transforming previously asymmetric channels into even-parity configurations under spatial inversion.

Our findings reveal that NH physics remarkably change the behavior of dynamical quantum properties in magnetic systems, as also pointed out in Ref. [68]. The effective coupling between the ferromagnetic lead and the AM/UM, characterized by Γ, γ, is theoretically controlled by manipulating the spin-dependent density of states. From an experimental standpoint, the strength of these couplings corresponds to physical setups where a thin potential tunneling barrier is inserted between both systems [69], including an oxygen gradient [70] or where an auxiliary electron reservoir is implemented to modulate the nonconservative particle exchange [41,71]. In our theoretical framework, following the open-quantum-system approach detailed by [41], we model these AM (UM) / FM lead junctions by explicitly integrating out the degrees of freedom of the reservoir. This procedure yields the NH effective Hamiltonian through the frequency-independent retarded self-energy evaluated at the Fermi level, consistent with the transport models discussed in Ref. [72]. Within this framework, the damping of the physical signals arises naturally from the nonconservative exchange with the environment, in a manner analogous to the dissipative regimes reported in Josephson junctions [71]. Regarding our choice for parameters, phenomenologically, $\gamma \approx 0.05t$ (corresponding to $\sim$50 meV for a typical metallic hopping $t \sim 1$ eV) would be related to lifetime broadening usually encountered in metallic magnetic heterostructures due to interface disorder, electron-phonon scattering, spin fluctuations, and hybridization across the interface, even at room temperature [73]. In altermagnet/ferromagnet interfaces (e.g., RuO_2 /Co or MnTe/Fe), this broadening remains significantly smaller than the characteristic altermagnetic spin splitting ($\alpha \sim 0.1 - 1$ eV), placing the system in the experimentally relevant regime $\gamma/\alpha \ll 1$, where non-Hermitian effects can coexist with well-resolved spin-split bands. Given the recent experimental confirmation of the large altermagnetic spin-splitting in materials such as MnTe [3] or $LuFeO_3$, which was reported to present a transverse spin susceptibility as large as $0.5\hbar$ Å/V without NH features [24], clearly, based on our study, we provide a realistic pathway for the experimental realization of spin-charge conversion devices where dissipation acts as a functional tuning parameter, and this value is expected to decrease in an open environment. Similarly, CeNiAsO serves as a material that shows a p-wave order capable of reaching large REE efficiencies in the absence of SOC where the theoretically estimated $\chi_{yx} \approx 13\,\hbar\,\text{Å}/\text{V}$ might be reduced to 70% of its value after considering NH effects, and at the same time, a parallel component of the spin susceptibility should also be expected.

ACKNOWLEDGMENTS

The authors thank A. Manchon for helpful discussions and suggestions. This work was supported by the Japan Science and Technology Agency (JST) ASPIRE Program No. JPMJAP2410, the ANR 'ORION' project, Grant No. ANR-20-CE30-0022-01 of the French Agence Nationale de la Recherche, ANR-22-CE30-0026 'DYNTOP' project, by a France 2030 government grant managed by the French National Research Agency PEPR SPIN ANR-22-EXSP0009 'SPINTHEORY', and by the program "Excellence Initiative - research university" for AGH University of Krakow.

DATA AVAILABILITY

There are no publicly available research data or software supporting this manuscript. Requests for further information or data should be sent to the authors.

APPENDIX A: EXPANSION IN TAYLOR SERIES AND PARITY SELECTION RULES FOR d_{xy}- WAVE AM

To evaluate the emergence of the spin accumulation given by the integral of Eq. (9), we expand the analytical traces as a Taylor series. For the d_{xy}-wave AM with Néel vector $\mathbf{n} \parallel z$, the expression from Eq. (9) can be decomposed by isolating the even parity of the denominator, i.e., $\mathcal{D}_{\text{par}} = -16\alpha^2 k_x^2 k_y^2 E^6 + \gamma^2 B + Q + E^8$, from the odd-parity altermagnetic term $\mathcal{D}_{\text{impar}} = 32\alpha\eta\gamma k_x k_y E^5$. By applying a geometric series expansion to the denominator, $\mathcal{D}^{-1} = (\mathcal{D}_{\text{par}} + \mathcal{D}_{\text{impar}})^{-1} \approx \mathcal{D}_{\text{par}}^{-1} - \mathcal{D}_{\text{impar}}\mathcal{D}_{\text{par}}^{-2}$, the full trace expands to lowest order as

$$\text{Tr}^{d_{xy}} \approx \gamma \frac{\mathcal{N}_1}{\mathcal{D}_{\text{par}}} - \gamma \frac{\mathcal{N}_1 \mathcal{D}_{\text{impar}}}{\mathcal{D}_{\text{par}}^2} + O(\gamma^3, \mathbf{k}^5), \tag{A1}$$

where $\mathcal{N}_1 = -192\alpha\eta k_x^2 k_y^2 \lambda_R^3 E - 64\alpha\eta k_y^2 \lambda_R E^3$. An inspection of Eq. (A1) justifies the physical responses discussed in Sec. III C 1.

(1) *First term* ($\gamma \frac{\mathcal{N}_1}{\mathcal{D}_{\text{par}}}$): Since $\mathcal{D}_{\text{par}}$ is symmetric under individual axial reflections ($k_i \rightarrow -k_i$), the parity of this channel is determined solely by the numerator. The monomials within $\mathcal{N}_1$ are proportional to $k_x^2 k_y^2$ and k_y^2, rendering them strictly even in momentum space. Therefore, this baseline channel bypasses the full-zone cancellation and leads to the finite χ_{xx} response.

(2) *Second term* ($-\gamma \frac{\mathcal{N}_1 \mathcal{D}_{\text{impar}}}{\mathcal{D}_{\text{par}}^2}$): This cross-coupling combines the even numerator with the odd altermagnetic denominator contribution ($\mathcal{D}_{\text{impar}} \propto k_x k_y$). The resulting product is proportional to $k_x^3 k_y^3$ and $k_x k_y^3$, which are strictly odd functions that integrate identically to zero over the Brillouin zone.

This systematic analysis ensures that the macroscopic spin accumulation is governed by the even-parity channels unlocked by the competition between the altermagnetic parameter α and the NH parameter γ, confirming that higher-order expansion terms do not restore the vanishing behavior. On the other hand, inspecting the numerator for the $d_{x^2-y^2}$-wave AM in Eq. (11) gives an odd function of momentum. A similar parity analysis demonstrates that the full-zone integration vanishes identically, rendering the macroscopic χ_{xx} response null in this case.

APPENDIX B: VERTEX CORRECTION AND IMPACT OF DISORDER

Since disorder is ubiquitous in materials, we comment briefly on its impact by considering the standard expression $V(\mathbf{r}) = V_0 \sum_i \alpha(\mathbf{r} - \mathbf{r}_i)$ accounting for a nonmagnetic potential distributed in random points $\mathbf{r}_i$. In this sense, we restrict our analysis to the correction of the spin operator $\hat{s}_y$, appearing in the velocity operator $(\partial\varepsilon_{n,\mathbf{k}}/\partial k_x)$, by solving the Bethe-Salpeter equation in the ladder approximation [74],

$$\tilde{s}_y = \hat{s}_y + n_i V_0 \sum_k G^A(\mathbf{k}, E)\tilde{s}_y G^R(\mathbf{k}, E), \tag{B1}$$

where n_i is the density of impurities and V_0 is the potential strength taken as a constant through the whole sample. The low-energy dressed Hermitian GF is evaluated at the energy

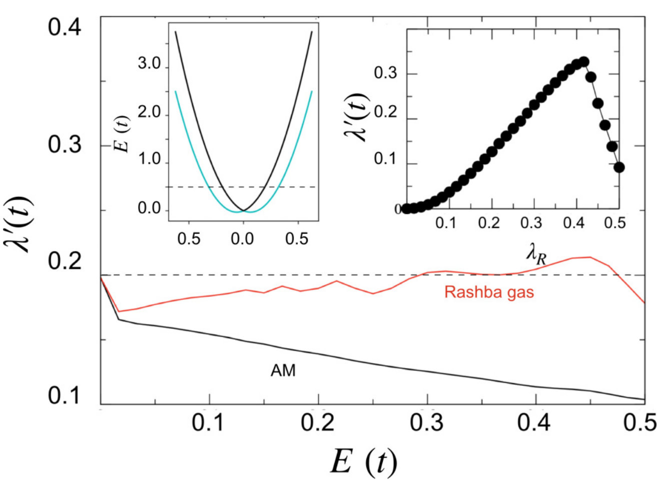

FIG. 6. Correction to the parameter λ_R denoted as λ' obtained from the vertex corrections when considering an impurity potential of 0.01t as a function of the Fermi level. Each of them was obtained by considering the full altermagnet Hamiltonian having $\alpha = 0.15t$ and $\lambda_R = 0.2t$ (black) and the pure Rashba Hamiltonian ($\alpha = 0$) (red), where interesting features are displayed as the monotonic behavior of the black curve directly related to the existence of a Rashba effect in an altermagnet. In contrast, the red curve shows an almost constant behavior accounting for the exact cancellation of the velocity operator in the case of the Rashba case. The inset displays the band structure of the full model along the k_x direction (left) and the modification of the correction λ' as the value of the Rashba parameter is modified on the right-hand side.

E corresponding to the long-wavelength limit ($|\mathbf{k}| \to 0$) of the Hamiltonian $[H_{kp}(\mathbf{k})]$ derived from Eq. (2) with $\Gamma = \gamma = 0$. For solving such a system, we assume a recursive procedure where the spin operators are written on the same basis of the Hamiltonian considered above, arriving at the following expression:

$$G^{R/A}(\mathbf{k}, E_F) = \frac{1}{E_F - H_{kp}(\mathbf{k}) \pm i\eta}. \tag{B2}$$

Then by plugging it into Eq. (B1), we calculate the corrections to the coefficient λ_R, labeled as λ', which is displayed in Fig. 6 for an energy window surrounding band crossing.

Unlike the k-independent velocity $\propto \sigma_y$ of the ferromagnetic Rashba gas, our system exhibits an out-of-plane velocity component due to the helicity of the altermagnet with anisotropic spin-split bands. As shown in Fig. 6, this modifies the spin operator σ_y. The black curve (for AM coupling $0.15t$) shows a correction that depends on λ_R, reaching a maximum near $0.4t$ and then decreasing toward zero as λ_R increases. This contrasts with the usual Rashba gas, where cancellation in $\partial H_R/\partial k_x \sim \sigma_y(\lambda_R - \lambda') = 0$ yields the standard result [75,76]. On the other hand, by considering the effective d-wave AM Hamiltonian Eq. (2) with $\theta = 0$, the velocity operator $\partial H_{AM}/\partial k_z$ includes a term $\propto \alpha k_y \sigma_z$, preventing this cancellation, and then leading to a qualitatively different behavior. This analysis has been reported already in the context of the anomalous and spin Hall effect in AMs [77]. In such a case, however, the correction diminishes away from the band-crossing point (the so called Dirac point), suggesting only a moderate or small effect on the full NH response as such corrections enter into Eq. (3) modifying the velocity operator.

[1] L. Šmejkal, J. Sinova, and T. Jungwirth, Beyond conventional ferromagnetism and antiferromagnetism: A phase with nonrelativistic spin and crystal rotation symmetry, Phys. Rev. X **12**, 031042 (2022).

[2] L. Šmejkal, J. Sinova, and T. Jungwirth, Emerging research landscape of altermagnetism, Phys. Rev. X **12**, 040501 (2022).

[3] J. Krempaský, L. Šmejkal, S. W. D'Souza, M. Hajlaoui, G. Springholz, K. Uhlířová, F. Alarab, P. C. Constantinou, V. Strocov, D. Usanov, W. R. Pudelko, R. González-Hernández, A. Birk Hellenes, Z. Jansa, H. Reichlová, Z. Šobáň, R. D. Gonzalez Betancourt, P. Wadley, J. Sinova, D. Kriegner, *et al.*, Altermagnetic lifting of Kramers spin degeneracy, Nature (London) **626**, 517 (2024).

[4] C. Song, H. Bai, Z. Zhou, L. Han, H. Reichlova, J. H. Dil, J. Liu, X. Chen, and F. Pan, Altermagnets as a new class of functional materials, Nat. Rev. Mater. **10**, 473 (2025).

[5] R. Xu, Y. Gao, and J. Liu, Chemical design of monolayer altermagnets, Natl. Sci. Rev. **13**, nwaf528 (2026).

[6] S. Sheoran and P. Dev, Spontaneous anomalous Hall effect in two-dimensional altermagnets, Phys. Rev. B **111**, 184407 (2025).

[7] E. Schwartz, H. Vakili, and A. A. Kovalev, Thermomagnonic torques in insulating altermagnets, arXiv:2512.14660.

[8] D. Wang, M.-D. He, L. Liu, and L.-M. Tang, Rashba–edelstein effect in altermagnetic twisted bilayers, Nanotechnology **37**, 065201 (2026).

[9] R. González-Hernández, P. Ritzinger, K. Výborný, J. Železný, and A. Manchon, Non-relativistic torque and Edelstein effect in non-collinear magnets, Nat. Commun. **15**, 7663 (2024).

[10] M. Trama, I. Gaiardoni, C. Guarcello, J. I. Facio, A. Maiellaro, F. Romeo, R. Citro, and J. van den Brink, Nonlinear anomalous Edelstein response at altermagnetic interfaces, Phys. Rev. B **112**, 184404 (2025).

[11] M. Yarmohammadi, J. Linder, and J. K. Freericks, Slow-phonon control of spin Edelstein effect in Rashba d-wave altermagnets, Phys. Rev. B **113**, 184403 (2026).

[12] M. Yarmohammadi, M. Berritta, M. Bukov, L. Šmejkal, J. Linder, and P. M. Oppeneer, Spin polarization engineering in d-wave altermagnets, Phys. Rev. B **113**, L060403 (2026).

[13] M. Ezawa, Detecting the Néel vector of altermagnets in heterostructures with a topological insulator and a crystalline valley-edge insulator, Phys. Rev. B **109**, 245306 (2024).

[14] K. Maeda, Y. Fukaya, K. Yada, B. Lu, Y. Tanaka, and J. Cayao, Classification of pair symmetries in superconductors with unconventional magnetism, Phys. Rev. B **111**, 144508 (2025).

[15] T. Kokkeler, I. Tokatly, and F. S. Bergeret, Quantum transport theory for unconventional magnets: Interplay of altermagnetism and p-wave magnetism with superconductivity, SciPost Phys. **18**, 178 (2025).

[16] B. Lu, K. Maeda, H. Ito, K. Yada, and Y. Tanaka, φ Josephson junction induced by altermagnetism, Phys. Rev. Lett. **133**, 226002 (2024).

[17] C. W. J. Beenakker and T. Vakhtel, Phase-shifted Andreev levels in an altermagnet Josephson junction, Phys. Rev. B **108**, 075425 (2023).

[18] J. A. Ouassou, A. Brataas, and J. Linder, DC Josephson effect in altermagnets, Phys. Rev. Lett. **131**, 076003 (2023).

[19] S. Banerjee and M. S. Scheurer, Altermagnetic superconducting diode effect, Phys. Rev. B **110**, 024503 (2024).

[20] H.-Y. Ma, M. Hu, N. Li, J. Liu, W. Yao, J.-F. Jia, and J. Liu, Multifunctional antiferromagnetic materials with giant piezomagnetism and noncollinear spin current, Nat. Commun. **12**, 2846 (2021).

[21] S. Das, D. Suri, and A. Soori, Transport across junctions of altermagnets with normal metals and ferromagnets, J. Phys.: Condens. Matter **35**, 435302 (2023).

[22] A. Birk Hellenes, T. Jungwirth, R. Jaeschke-Ubiergo, A. Chakraborty, J. Sinova, and L. Šmejkal, P-wave magnets, arXiv:2309.01607.

[23] S. Bhowal and A. Bose, Non-relativistic spin splitting: Features and functionalities, npj Quantum Mater. (2026).

[24] A. Chakraborty, A. Birk Hellenes, R. Jaeschke-Ubiergo, T. Jungwirth, L. Šmejkal, and J. Sinova, Highly efficient non-

relativistic Edelstein effect in nodal p-wave magnets, Nat. Commun. **16**, 7270 (2025).
[25] M. Ezawa, Out-of-plane Edelstein effects: Electric field induced magnetization in p-wave magnets, Phys. Rev. B **111**, L161301 (2025).
[26] A. A. Hedayati and M. Salehi, Transverse spin current at normal-metal/p-wave magnet junctions, Phys. Rev. B **111**, 035404 (2025).
[27] B. Brekke, P. Sukhachov, H. G. Giil, A. Brataas, and J. Linder, Minimal models and transport properties of unconventional p-wave magnets, Phys. Rev. Lett. **133**, 236703 (2024).
[28] K. Maeda, B. Lu, K. Yada, and Y. Tanaka, Theory of tunneling spectroscopy in unconventional p-wave magnet-superconductor hybrid structures, J. Phys. Soc. Jpn. **93**, 114703 (2024).
[29] Y. Fukaya, K. Yada, and Y. Tanaka, p-wave superconductivity and Josephson current in p-wave unconventional magnet/s-wave superconductor hybrid systems, Phys. Rev. B **114**, 014503 (2026).
[30] P. Sukhachov, H. G. Giil, B. Brekke, and J. Linder, Coexistence of p-wave magnetism and superconductivity, Phys. Rev. B **111**, L220403 (2025).
[31] M. Khodas, L. Šmejkal, and I. I. Mazin, Nonrelativistic-Ising superconductivity in p-wave magnets, Phys. Rev. B **114**, L080505 (2026).
[32] A. Manchon, J. Železný, I. M. Miron, T. Jungwirth, J. Sinova, A. Thiaville, K. Garello, and P. Gambardella, Current-induced spin-orbit torques in ferromagnetic and antiferromagnetic systems, Rev. Mod. Phys. **91**, 035004 (2019).
[33] Y. Ashida, Z. Gong, and M. Ueda, Non-Hermitian physics, Adv. Phys. **69**, 249 (2020).
[34] Z. Gong, Y. Ashida, K. Kawabata, K. Takasan, S. Higashikawa, and M. Ueda, Topological phases of non-Hermitian systems, Phys. Rev. X **8**, 031079 (2018).
[35] E. J. Bergholtz, J. C. Budich, and F. K. Kunst, Exceptional topology of non-Hermitian systems, Rev. Mod. Phys. **93**, 015005 (2021).
[36] X. Zhang, T. Zhang, M.-H. Lu, and Y.-F. Chen, A review on non-Hermitian skin effect, Adv. Phys.: X **7**, 2109431 (2022).
[37] K. Yokomizo and S. Murakami, Non-Bloch band theory of non-Hermitian systems, Phys. Rev. Lett. **123**, 066404 (2019).
[38] K. Kawabata, K. Shiozaki, M. Ueda, and M. Sato, Symmetry and topology in non-Hermitian physics, Phys. Rev. X **9**, 041015 (2019).
[39] N. Okuma and M. Sato, Non-Hermitian topological phenomena: A review, Annu. Rev. Condens. Matter Phys. **14**, 83 (2023).
[40] S. Manna and B. Roy, Inner skin effects on non-Hermitian topological fractals, Commun. Phys. **6**, 10 (2023).
[41] J. Cayao, Exceptional degeneracies in non-Hermitian Rashba semiconductors, J. Phys.: Condens. Matter **35**, 254002 (2023).
[42] M. Yang and C. H. Lee, Beyond the non-Hermitian skin effect: Scaling-controlled topology from exceptional-bound bands, Adv. Sci. **13**, e23989 (2026).
[43] G. K. Dash, S. Panda, and S. Nandy, Fingerprint of non-Hermiticity in a d-wave altermagnet, Phys. Rev. B **111**, 155119 (2025).
[44] M. A. Reja and A. Narayan, Emergence of tunable exceptional points in altermagnet-ferromagnet junctions, Phys. Rev. B **110**, 235401 (2024).
[45] M. Alipourzadeh, D. Afshar, and Y. Hajati, Opto- and magneto-tunable exceptional degeneracies in non-Hermitian ferromagnet/p-wave magnet junctions, Scientific Rep. (2026).
[46] M. A. Reja and A. Narayan, Néel vector controlled exceptional contours in p-wave magnet-ferromagnet junctions, New J. Phys. **27**, 092001 (2025).
[47] H. Isobe and N. Nagaosa, Anomalous Hall effect from a non-Hermitian viewpoint, Phys. Rev. B **107**, L201116 (2023).
[48] Y. Chen and H. Zhai, Hall conductance of a non-Hermitian Chern insulator, Phys. Rev. B **98**, 245130 (2018).
[49] A. Anadón, A. Pezo, I. Arnay, R. Guerrero, A. Gudín, A. Guio, M. Yactayo, J. Ghanbaja, J. Camarero, A. Manchon, S. Petit-Watelot, P. Perna, and J. Rojas-Sánchez, Giant and anisotropic enhancement of spin-charge conversion in graphene-based quantum system, Adv. Mater. **37**, 2418541 (2025).
[50] K.-i. Uchida, H. Adachi, T. Kikkawa, A. Kirihara, M. Ishida, S. Yorozu, S. Maekawa, and E. Saitoh, Thermoelectric generation based on spin Seebeck effects, Proc. IEEE **104**, 1946 (2016).
[51] M. Sung, S.-R. Moon, E.-S. Kim, S. Cho, J. K. Lee, S.-H. Cho, T. Kawanishi, and H.-J. Song, Design considerations of photonic THz communications for 6G networks, IEEE Wireless Commun. **28**, 185 (2021).
[52] R. Rouzegar, A. L. Chekhov, Y. Behovits, B. R. Serrano, M. A. Syskaki, C. H. Lambert, D. Engel, U. Martens, M. Münzenberg, M. Wolf, G. Jakob, M. Kläui, T. S. Seifert, and T. Kampfrath, Broadband spintronic terahertz source with peak electric fields exceeding 1.5 mV/cm, Phys. Rev. Appl. **19**, 034018 (2023).
[53] A. Pezo, S. Massabeau, F. Miljević, J.-M. George, H. Jaffrès, J. Li, F. Ibrahim, M. Jamet, and M. Chshiev, Spin and orbital Rashba response in ferroelectric polarized $PtSe_2/MoSe_2/LiNbO_3$ heterostructures, Phys. Rev. Appl. **25**, 054027 (2026).
[54] X.-P. Zhang, W. Feng, R.-W. Zhang, X. Fan, X. Wang, and Y. Yao, Theory of anisotropic magnetoresistance in altermagnets and its applications, Phys. Rev. Lett. **135**, 266706 (2025).
[55] R. Capecelatro, M. Marciani, G. Campagnano, R. Citro, and P. Lucignano, Supercurrent from the imaginary part of the Andreev levels in non-Hermitian Josephson junctions, Phys. Rev. B **113**, 184506 (2026).
[56] C. Payá, O. Solow, E. Prada, R. Aguado, and K. Flensberg, Non-Hermitian skin effect and electronic nonlocal transport, Phys. Rev. B **113**, L161405 (2026).
[57] D. Zhu, Z.-Y. Zhuang, Z. Wu, and Z. Yan, Topological superconductivity in two-dimensional altermagnetic metals, Phys. Rev. B **108**, 184505 (2023).
[58] P. Rao, A. Mook, and J. Knolle, Tunable band topology and optical conductivity in altermagnets, Phys. Rev. B **110**, 024425 (2024).
[59] Y. Yu, M. B. Lyngby, T. Shishidou, M. Roig, A. Kreisel, M. Weinert, B. M. Andersen, and D. F. Agterberg, Odd-parity magnetism driven by antiferromagnetic exchange, Phys. Rev. Lett. **135**, 046701 (2025).
[60] X.-M. Zhao, C.-X. Guo, X.-R. Ma, X.-R. Wang, and S.-P. Kou, Tailoring corner states and exceptional points in altermagnets, Phys. Rev. B **113**, L100409 (2026).
[61] V. Bonbien and A. Manchon, Symmetrized decomposition of the Kubo-Bastin formula, Phys. Rev. B **102**, 085113 (2020).

[62] D. García Ovalle, A. Pezo, and A. Manchon, Spin-orbit torque for field-free switching in C_{3v} crystals, Phys. Rev. B **107**, 094422 (2023).
[63] A. Pezo *et al.*, Ferroelectric control of spin and orbital Rashba effects at the Ni/HfO_2 interface, Phys. Rev. B **111**, L140405 (2025).
[64] A. Pezo *et al.*, Theory of spin and orbital charge conversion at the surface states of $Bi_{1-x}Sb_x$ topological insulator, Phys. Rev. Res. **6**, 043332 (2024).
[65] B. Michen and J. C. Budich, Mesoscopic transport signatures of disorder-induced non-Hermitian phases, Phys. Rev. Res. **4**, 023248 (2022).
[66] M. R. Hirsbrunner, T. M. Philip, and M. J. Gilbert, Topology and observables of the non-Hermitian Chern insulator, Phys. Rev. B **100**, 081104(R) (2019).
[67] F. K. Kunst and V. Dwivedi, Non-Hermitian systems and topology: A transfer-matrix perspective, Phys. Rev. B **99**, 245116 (2019).
[68] H. M. Hurst and B. Flebus, Non-Hermitian physics in magnetic systems, J. Appl. Phys. **132**, 220902 (2022).
[69] B. Flebus, R. A. Duine, and H. M. Hurst, Non-Hermitian topology of one-dimensional spin-torque oscillator arrays, Phys. Rev. B **102**, 180408(R) (2020).
[70] X. Feng, T. Wu, Z. Gao, H. Zhao, S. Wu, Y. Zhang, L. Ge, and L. Feng, Non-Hermitian hybrid silicon photonic switching, Nat. Photon. **19**, 264 (2025).
[71] J. Qi, M. Lu, J. Liu, C.-Z. Chen, and X. C. Xie, Non-Hermitian superconducting diode effect, Phys. Rev. B **112**, L060502 (2025).
[72] A. V. Gordeeva, A. L. Pankratov, N. G. Pugach, A. S. Vasenko, V. O. Zbrozhek, A. V. Blagodatkin, D. A. Pimanov, and L. S. Kuzmin, Record electron self-cooling in cold-electron bolometers with a hybrid superconductor-ferromagnetic nanoabsorber and traps, Sci. Rep. **10**, 21961 (2020).
[73] M. C. T. D. Müller, S. Blügel, and C. Friedrich, Electron-magnon scattering in elementary ferromagnets from first principles: Lifetime broadening and band anomalies, Phys. Rev. B **100**, 045130 (2019).
[74] J. Q. Li and C. M. Wang, Edelstein effect in pseudospin Dirac systems, Phys. Rev. B **103**, 085401 (2021).
[75] J.-i. Inoue, T. Kato, Y. Ishikawa, H. Itoh, G. E. W. Bauer, and L. W. Molenkamp, Vertex corrections to the anomalous Hall effect in spin-polarized two-dimensional electron gases with a Rashba spin-orbit interaction, Phys. Rev. Lett. **97**, 046604 (2006).
[76] J.-i. Inoue, G. E. W. Bauer, and L. W. Molenkamp, Suppression of the persistent spin Hall current by defect scattering, Phys. Rev. B **70**, 041303(R) (2004).
[77] W. Chen, L. Zeng, and W. Zhu, Helicity-controlled spin Hall angle in 2D altermagnets with Rashba spin-orbit coupling, Chinese Phys. Lett. **42**, 017201 (2025).